ENDOR Structural Characterization of a Catalytically Competent Acylenzyme Reaction Intermediate of Wild-Type TEM-1 β-Lactamase Confirms Glutamate-166 as the Base Catalyst†

Devkumar Mustafi, Alejandro Sosa-Peinado,‡ and Marvin W. Makinen*

Department of Biochemistry and Molecular Biology, The University of Chicago, Cummings Life Science Center, 920 East 58th Street, Chicago, Illinois 60637

Received September 7, 2000; Revised Manuscript Received December 1, 2000

ABSTRACT: The catalytically competent active-site structure of a true acylenzyme reaction intermediate of TEM-1 β-lactamase formed with the kinetically specific spin-labeled substrate 6-*N*-(2,2,5,5-tetramethyl-1-oxypyrrolinyl-3-carboxyl)-penicillanic acid isolated under cryoenzymologic conditions has been determined by angle-selected electron nuclear double resonance (ENDOR) spectroscopy. Cryoenzymologic experiments with use of the chromophoric substrate 6-*N*-[3-(2-furanyl)-propen-2-oyl]-penicillanic acid showed that the acylenzyme reaction intermediate could be stabilized in the −35 to −75 °C range with a half-life suitably long to allow freeze-quenching of the reaction species for ENDOR studies while a noncovalent Michaelis complex could be optically identified at temperatures only below −70 °C. The wild-type, Glu166Asn, Glu240Cys, and Met272Cys mutant forms of the mature enzyme were overexpressed in perdeuterated minimal medium to allow detection and assignment of proton resonances specific for the substrate and chemically modified amino acid residues in the active site. From analysis of the dependence of the ENDOR spectra on the setting of the static laboratory magnetic field $\mathbf{H}_0$, the dipolar contributions to the principal hyperfine coupling components were estimated to calculate the separations between the unpaired electron of the nitroxyl group and isotopically identified nuclei. These electron−nucleus distances were applied as constraints to assign the conformation of the substrate in the active site and of amino acid side chains by molecular modeling. Of special interest was that the ENDOR spectra revealed a water molecule sequestered in the active site of the acylenzyme of the wild-type protein that was not detected in the deacylation impaired Glu166Asn mutant. On the basis of the X-ray structure of the enzyme, the ENDOR distance constraints placed this water molecule within hydrogen-bonding distance to the carboxylate side chain of glutamate-166 as if it were poised for nucleophilic attack of the scissile ester bond. The ENDOR results provide experimental evidence of glutamate-166 in its functional role as the general base catalyst in the wild-type enzyme for hydrolytic breakdown of the acylenzyme reaction intermediate of TEM-1 β-lactamase.

The mechanism of action of β-lactamases as a major source of penicillin-based antibiotic resistance in bacteria remains conjectural despite the discovery of penicillin over 70 years ago (*1*). The most prevalent of the four classes of β-lactamases are the class A and class C enzymes that are evolutionarily related and function as serine hydrolases (*2*, *3*). Salient aspects of the reaction that they catalyze are highlighted in the upper part of Figure 1. A number of class A and class C β-lactamases have been characterized by X-ray crystallography at high resolution (*4*, *5*). However, relatively little is known about the structural basis for variability in mechanism, and only the catalytic role of the active-site serine residue as a nucleophile is unambiguously resolved. In analogy to the serine proteases, it is anticipated that proton abstraction to potentiate the serine hydroxyl group for nucleophilic attack in acylation and activation of a water molecule for cleavage of the acylenzyme occur as general base-catalyzed processes. However, it is unresolved whether one or two different residues are involved in catalyzing acylation and deacylation steps. In addition, spatial variability in the sequestering of the hydrolytic water for cleavage of the acylenzyme reaction intermediate may be an important factor contributing to mechanistic differences between the class A and class C enzymes (*6*).

To understand the molecular basis of enzyme function, as schematically represented in Figure 1A, it is necessary to determine the kinetic and thermodynamic parameters governing each step of the enzyme-catalyzed reaction, the structures of reaction intermediates and of the free substrate and product, and the time-dependent atomic rearrangements involving the substrate and the enzyme. The main obstacle to determining structures of reaction intermediates stems from the rapidity of enzyme catalytic action itself. For these reasons enzyme mechanisms are generally inferred on the basis of X-ray determined structures of enzyme−inhibitor complexes or on the basis of enzyme−substrate complexes in which the enzyme has been rendered catalytically impaired through genetic manipulation. Since nonproductive structural

† This work was supported by a grant of the National Institutes of Health (GM21900).

* To whom correspondence should be addressed. E-mail: makinen@uchicago.edu.

‡ Present address: Department of Biochemistry, School of Medicine, National Autonomous University of Mexico, Mexico, D. F., 04510.

10.1021/bi0021075 CCC: $20.00
Published on Web 01/27/2001

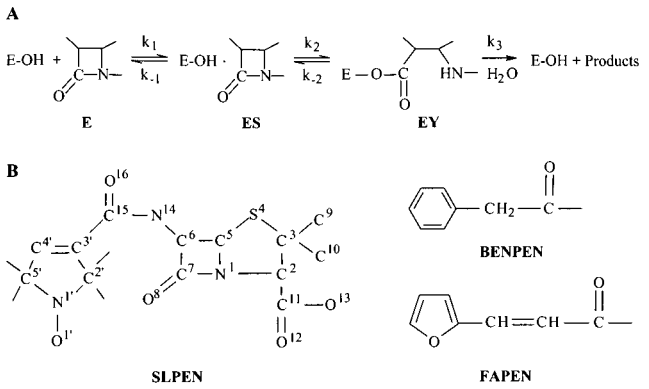

FIGURE 1: (A) Illustration of the hydrolytic reaction underlying the interaction of penicillin-binding enzymes of the serine hydrolase classes with β-lactam antibiotics. Formation of the Michaelis complex (ES) is followed by proton abstraction from the serine hydroxyl group to potentiate nucleophilic attack for acylenzyme (EY) formation. Hydrolytic breakdown of the EY intermediate leads to destruction of the antibiotic potency of the β-lactam compound. For β-lactamases, k_3, governing the rate-limiting step, can be very high, even of the order of $\sim$2000 s^{-1} as for TEM-1 β-lactamase while for the DD-peptidase, which represents the target enzyme of the antibiotic, k_3 is very low ($\leq 10^{-3}$ s^{-1}). (B) Atomic numbering scheme of the spin-labeled penicillin 6-*N*-(2,2,5,5-tetramethyl-1-oxypyrrolinyl-3-carboxyl)-penicillanic acid (SLPEN) employed as the spectroscopic probe substrate in this study. To the right of the atomic numbering scheme for SLPEN, we have illustrated for comparative purposes the chemical bonding structures of the acylamido groups of BENPEN and of FAPEN, both of which are employed as substrates of TEM-1 β-lactamase in this study. The carbonyl group in each corresponds to the C(15)═O(16) group in SLPEN and represents the point of covalent attachment to the N(14) atom of the 6-amino-penicillanic acid moiety.

relationships are responsible for the long-term stability of such complexes, the observed structures revealed through such diffraction experiments cannot possess the complete set of enzyme:substrate interactions required for the catalytic conversion of substrate to product.

We have shown through a series of studies published from this laboratory that application of electron nuclear double resonance (ENDOR)[1] spectroscopy for structure analysis of true, catalytically competent intermediates of enzyme catalyzed reactions provides an incisive means to identify and structurally characterize enzyme:substrate interactions that are catalytically important and are not observed in enzyme−inhibitor complexes (*7*−*10*). We have applied this approach to characterize the acylenzyme reaction intermediate of TEM-1 β-lactamase, using a kinetically specific, nitroxyl spin-labeled penicillin (*11*, *12*) as a paramagnetic probe of active-site structure. In addition to assigning the catalytically competent conformation of the acyl moiety of the substrate in the acylenzyme reaction intermediate, we have extended this approach through site-directed cysteine mutagenesis to assign structural relationships of nearby active-site residues. By comparative ENDOR spectroscopy of the reaction intermediates of the wild-type enzyme and of the deacylation impaired Glu166Asn mutant (*13*, *14*), we have identified a sequestered water molecule in the active site of the wild-type enzyme within hydrogen-bonding distance to the carboxylate group of the glutamate-166 residue, positioned as if it were poised for nucleophilic attack on the scissile ester bond in the acylenzyme. This water molecule is not detected in the acylenzyme formed with the Glu166Asn mutant. The ENDOR results provide direct support of glutamate-166 in its functional role as the general base catalyst for hydrolytic cleavage of the acylenzyme reaction intermediate in wild-type TEM-1 β-lactamase. In conjunction with the pH dependence of the steady-state kinetic parameters k_{cat} and k_{cat}/K_M governing the hydrolysis of substrates (*12*, *15*, *16*) and simulation of electrostatic interactions governing the catalytic reaction (*17*), these results suggest further that only one active-site residue, glutamate-166 with its carboxylate side chain, functions as the general base catalyst in both acylation and deacylation processes.

METHODS AND MATERIALS

General. BENPEN (Sigma Chemical Co., St. Louis, MO 63178) and FAPEN (Calbiochem, La Jolla, CA 92039) were used without further purification upon purchase. The spin-labeled substrate SLPEN was synthesized as described previously and all analytical data indicated comparable purity to that reported earlier (*11*). Deuterated solvents and sodium [$^2H_3$]acetate ($\geq$99% ^2H) were purchased from Cambridge Isotope Laboratories, Inc. (Woburn, MA 01801). All other reagents were of analytical reagent grade, and deionized distilled water was used throughout.

Wild-Type and Mutant Forms of TEM-1 β-Lactamase. A detailed description for overexpression, deuterium enrichment, creation of point mutations, and purification of recombinant TEM-1 β-lactamase employed in this investigation has been published from this laboratory (*18*). Engineered *Escherichia coli* BL21 (DE3) cells were grown on LB medium and mature wt TEM-1 β-lactamase was recovered generally at a level of 140 mg/L. Growth of the engineered BL21 (DE3) cells on ^2H_2O and sodium [$^2H_3$]acetate (3 g/L) yielded $\geq$70 mg/L of mature wt protein enriched with deuterium to 88−90%, estimated by MALDI-TOF mass spectrometry. The Glu166Asn, Glu240Cys, and Met272Cys mutants were generated by application of the extended polymerase chain reaction (*19*), and the transformed BL21 (DE3) cells with the mutant gene were similarly grown on perdeuterated minimal medium.

Chemical Modification of the Enzyme. We have used two types of chemical modifications: (*i*) For the cysteine mutants Glu240Cys and Met272Cys, we treated the enzyme either with MMTS or [$^2H_3$]MMTS, synthesized according to literature procedures for the tritiated analogue (*20*), and (*ii*) For the acetylated enzyme, we treated the wt enzyme with acetylimidazole or [$^2H_3$]acetylimidazole, synthesized as described earlier (*8*). In each case, the reaction was carried out at 25 °C by using a 10-fold excess of ligand followed by extensive dialysis against buffer at 4 °C. The stoichiometry of chemically modified groups was determined by electrospray ionization mass spectrometry, and the results are presented below in conjunction with steady-state kinetic analysis of enzyme catalytic efficiency.

[1] Abbreviations: BENPEN, benzylpenicillin; CHES, 2-(*N*-cyclohexylamino)sulfonate; ENDOR, electron nuclear double resonance; EPR, electron paramagnetic resonance; FAPEN, 6-*N*-[3-(2-furanyl)-propen-2-oyl]-penicillanic acid; HEPES, *N*-(2-hydroxyethyl)piperazine-*N*′-2-ethanesulfonic acid; hf, hyperfine; hfc, hyperfine coupling; LB, Luria-Bertani; MALDI-TOF, matrix assisted laser desorption ionization time-of-flight; MES, 2-(*N*-morpholino)ethanesulfonate; MeOH, methanol; MMTS, methylmethanethiolsulfonate; PIPES, piperazine-*N*,*N*′-bis-(2-ethanesulfonate); SLPEN, 6-*N*-(2,2,5,5-tetramethyl-1-oxypyrrolinyl-3-carboxyl)-penicillanic acid or spin-labeled penicillin; wt, wild-type.

Enzyme Kinetics. Initial velocity data were collected spectrophotometrically to determine the steady-state kinetic parameters k_{cat} and k_{cat}/K_M for hydrolysis of penicillin substrates catalyzed by TEM-1 β-lactamase. Hydrolysis was followed by monitoring the change in absorbance at 232 nm for BENPEN ($\Delta\epsilon = 1015\ M^{-1}\ cm^{-1}$); at 230 nm for SLPEN ($\Delta\epsilon = 670\ M^{-1}\ cm^{-1}$); and at 325 nm for FAPEN ($\Delta\epsilon = 3019\ M^{-1}\ cm^{-1}$). Real-time data acquisition was carried out with use of a Cary 15 recording spectrophotometer modified by On-Line Instrument Systems, Inc. (Jefferson, GA 30549) and adapted with a stirring assembly and cryostat developed in this laboratory for collection of kinetic data in the ambient to −90 °C temperature range (*21*). Initial velocity data were evaluated with use of the nonlinear, least-squares algorithm ENZKIN, as described previously (*22*, *23*). For cryokinetic experiments, the pH* of cryosolvent mixtures was defined according to protocols of Douzou and co-workers (*24*, *25*).

EPR and ENDOR Spectroscopy. EPR and ENDOR spectra were recorded with use of an X-band Bruker ESP 300E spectrometer equipped with a TM_{110} cylindrical cavity, Bruker ENDOR accessory, and Oxford Instruments ESR910 liquid helium cryostat, as described previously (*26*, *27*). Typical experimental conditions for ENDOR measurements were as follows: sample temperature, 20 K; microwave frequency, 9.45 GHz; incident microwave power, 2 mW; modulation frequency, 12.5 kHz; and rf modulation depth, ~8 kHz.

For ENDOR spectroscopy, enzyme samples in EPR tubes were partially submerged in baths at different temperatures for controlled introduction of the organic solvent and substrate with a gastight, high-precision syringe equipped with a Teflon catheter (Hamilton Co., Reno, NV 89520). Typically a 0.3 mL solution of 1.0 M NaCl buffered to pH or pD 7.5 with 0.04 M sodium cacodylate and containing $(4.0-8.0) \times 10^{-4}$ M enzyme was brought to 0 °C in a water/ice bath for introduction of 8×0.01 mL aliquots of MeOH. Stirring of the solution was carried out after addition of each aliquot by movement of a thin stainless steel rod and loop submerged in the enzyme solution. The tube was then transferred to a bath at −18 °C (ethylene glycol/solid CO_2) for introduction of 11×0.01 mL aliquots of MeOH, similarly with stirring. The tube was finally transferred to a bath at −35 °C (xylene/solid CO_2) for addition of a 0.01 mL aliquot of SLPEN that had been freshly dissolved in methanol so that the enzyme:substrate ratio was 1.25:1.0 in a mixture of 40:60 (v/v) MeOH: H_2O. Mixing of the substrate with the enzyme in the cryosolvent required less than 30 s, and the temperature of the enzyme mixture was always confirmed with use of a copper−constantan thermocouple probe prior to injection of substrate. No precipitation of the protein was observed under these conditions. All samples were stored frozen in liquid nitrogen for spectroscopic data collection.

Molecular Modeling. The atomic numbering scheme of SLPEN is shown in Figure 1B. Graphics modeling of TEM-1 β-lactamase was carried out with use of INSIGHT95 (Biosym Technologies, Inc., 9685 Scranton Road, San Diego, CA 92121) running on an SGI R4400 Indigo^2 workstation with Solid Impact Graphics. Atomic coordinates of SLPEN were constructed from X-ray defined molecular fragments of 2,2,5,5-tetramethyl-1-oxypyrroline-3-carboxamide (*28*) and amoxycillin (*29*), as previously described (*9*, *11*). The atomic coordinates of TEM-1 β-lactamase were obtained from the Brookhaven Protein Data Bank (file 1BTL) for the free enzyme (*30*). Refined atomic coordinates of the benzylpenicilloyl-serine-70 acylenzyme of the Glu166Asn mutant (*14*) at 1.7 Å resolution were provided by Drs. N. C. J. Strynadka and M. N. G. James (personal communication). For molecular modeling of the acetylated form of TEM-1 β-lactamase, the X-ray structure of 2-acetoxy-3-methylbenzoic acid (*31*) was employed to construct tyrosine-105 into an acetyl tyrosinate residue. Also, for modeling the Glu240Cys and Met272Cys mutants of TEM-1 β-lactamase, a cysteine residue was first superpositioned onto the glutamate-240, viz., methionine-272 side chain, and the thiomethoxy (CH_3S-) group was attached to the sulfur atom of cysteine according to the X-ray structure of the mixed disulfide 2-desamino-L-cystine (*32*). Positions of idealized methyl hydrogen atoms were calculated for a tetrahedral carbon with use of SYBYL (Tripos Associates, Inc., 1600 S. Hanley Road, St. Louis, MO 63144).

To construct a molecular model of the spin-labeled penicilloyl-serine-70 acylenzyme reaction intermediate of wt TEM-1 β-lactamase, we employed the molecular model of methyl 6-*N*-(2,2,5,5-tetramethyl-1-oxypyrrolinyl-3-carboxyl)-penicilloate derived through ENDOR studies (*12*). This model was superpositioned onto the benzyl penicilloyl-serine-70 residue in the X-ray defined acylenzyme of the Glu166Asn mutant (*14*) so that the O_M-CH_3 bond vector of the methyl penicilloate molecule (*12*) coincided with the O^{γ}-$C^{\beta}H_2$ bond vector of the serine-70 residue in the active site of the acylenzyme. The ester O_M atom and CH_3 group were removed by editing the merged coordinate listings, preserving the same typical bond distance and valence angle parameters in the spin-labeled penicilloyl-serine-70 linkage, as are described for the benzyl penicilloyl acylenzyme of the Glu166Asn mutant (*14*). The penicilloyl moieties were then superposed so as to remove steric overlap with active-site residues while placing the 2-carboxylate group of the substrate into the anion binding site and the β-lactam C═O group into the oxyanion hole as in the Glu166Asn acylenzyme. Aside from the methyl ester group and the cleaved β-lactam bond, the structure of the spin-labeled methyl penicilloate ester differs from that of SLPEN primarily through the tetrahedral valence angles around C(6) and the value of the τ[N(1)−C(5)-C(6)−C(7)] torsion angle (*12*).

The asparagine-166 residue in the Glu166Asn mutant was replaced by a glutamate residue with the REPLACE option in INSIGHT95. The conformation of glutamate-166 was assigned as in the wt enzyme (*30*). Further torsional alteration of the spin-labeled penicilloyl-serine-70 moiety around rotatable bonds with application of ENDOR determined distance constraints was carried out within allowed intramolecular van der Waals conformational space of the spin-labeled substrate and allowed intermolecular van der Waals hard sphere contacts with active-site residues, as described in the text.

RESULTS AND DISCUSSION

Cryokinetic Isolation of Reaction Intermediates of TEM-1 β-Lactamase

Steady-State Kinetic Characterization of Wild-Type and Mutant Forms of TEM-1 β-Lactamase. In Figure 2 we

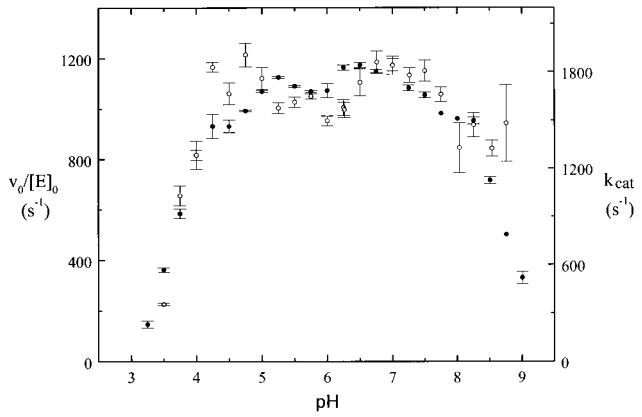

FIGURE 2: Comparison of the pH profiles of k_{cat} governing hydrolysis of benzylpenicillin and of v_0/E_0 for hydrolysis of SLPEN catalyzed by TEM-1 β-lactamase. The kinetic data were collected under initial velocity conditions for both substrates. The reaction mixture consisted of 0.1 M NaCl with the following buffers at 0.05 M concentration: pH 3.25−4.0, formate; pH 4.25−5.25, acetate; pH 5.5−6.0, MES; pH 6.2−7.0, PIPES; pH 7.2−8.2 HEPES; pH 8.5−9.2, CHES. For collection of v_0/E_0 data, the concentration of SLPEN was $\geq 2-3 \times K_M$, and the enzyme concentration was $8-10 \times 10^{-9}$ M. [(●) v_0/E_0 for SLPEN; (○) k_{cat} for BENPEN].

compare the pH profile of k_{cat} for hydrolysis of BENPEN to the pH profile of v_0/E_0 for hydrolysis of SLPEN catalyzed by the wt TEM-1 enzyme. Since we have not observed product or substrate inhibition for hydrolysis of the spin-labeled substrate, the pH profile of v_0/E_0 can be viewed essentially as a very close approximation of $k_{cat.}$ At pH 7.0, the values of the steady-state kinetic parameters for BENPEN and SLPEN were 1840 ± 20 and 1273 ± 29 s^{-1} for k_{cat} and $19.9 \pm 0.5 \times 10^6$ and $17.5 \pm 0.9 \times 10^6$ M^{-1} s^{-1} for k_{cat}/K_M, respectively. On this basis the kinetic specificity of SLPEN is as high for the TEM-1 enzyme as is that of the classical substrate BENPEN. Similar observations have been previously reported for the kinetic reactivity of SLPEN with the class A β-lactamase I and the class B zinc-containing β-lactamase II of *Bacillus cereus* (*11*, *12*).

The influence and stoichiometry of chemical modifications of active-site residues on steady-state kinetic properties are summarized in Table 1. While the kinetic specificity of the cysteine mutants and of their respective chemically modified forms, as measured by k_{cat}/K_M, was reduced compared to that of the wt enzyme, the change was comparable for both substrates, indicating that SLPEN experiences similar perturbations of active-site interactions as does the classical substrate BENPEN. The kinetic specificity of the Glu240Cys mutant is essentially equivalent to that of the wt enzyme while chemical modification with MMTS affects primarily k_{cat}. On the other hand, the Met272Cys mutant is associated with a change in both k_{cat} and K_M by a factor of ~2. Chemical modification of the Met272Cys mutant is seen to result in a further decrease in k_{cat}, as seen also for reaction of Glu240Cys with MMTS. Although these positions for introduction of cysteine residues were selected because they occur on the periphery of the active site at the solvent−protein interface (*14*, *30*), it is evident that they, nevertheless, experience steric interactions with the substrate when bound in the active site. Despite the decrease in kinetic specificity, the kinetic parameters, particularly as reflected by k_{cat}, indicate that the cysteine mutants and their chemically modified forms remain fully functional enzymes. While a larger value of K_M can be expected to decrease the fraction of noncovalent Michaelis complex detected in the very low, subzero temperature range compared to the native wt enzyme, formation of the acylenzyme reaction intermediate will be strengthened through the decrease in k_{cat} since breakdown of the acylenzyme intermediate remains rate limiting, as discussed below.

The kinetic specificity of acetyl-TEM-1 β-lactamase remains comparable to that of the native enzyme. Of the four tyrosine residues in the wt enzyme, the mass spectrometric results indicate that acetylation of 3.55 ± 0.11 residues/enzyme molecule has occurred on average. Nonetheless, the reactivity of the acetylated enzyme remains comparable to that of the native enzyme, probably because there is only one tyrosine residue in the active site and the hydroxyl group does not have steric contact with the substrate (*14*).

Cryokinetic Conditions for Accumulation of the Acylenzyme Reaction Intermediate. In separate experiments we have determined that the most suitable cryosolvent was MeOH

Table 1: Comparison of Steady-State Kinetic Parameters Governing the Hydrolysis of BENPEN and SLPEN Catalyzed by Wild-Type and Chemically Modified Mutants of TEM-1 β-Lactamase[a]

enzyme	molecular weight[b] (observed; theoretical)	k_{cat} (s^{-1})	K_M (10^{-6}, M)	k_{cat}/K_M (10^6, M^{-1} s^{-1})
wild-type	28 904 ± 3; 28 905	1840 ± 20	92 ± 2	19.9 ± 0.5
		1273 ± 29	73 ± 4	17.5 ± 1.0
Glu240Cys[c]	28 877 ± 7; 28 881	1597 ± 110	78 ± 8	20.5 ± 0.9
		1038 ± 12	96 ± 14	10.8 ± 1.1
Glu240Cys-SCH_3[d]	28 925 ± 5; 28 928	790 ± 44	103 ± 12	7.7 ± 1.1
		490 ± 28	120 ± 19	4.1 ± 0.9
Met272Cys	28 872 ± 7; 28 878	945 ± 87	215 ± 16	4.4 ± 1.0
		519 ± 49	225 ± 26	2.3 ± 0.8
Met272Cys-SCH_3[d]	28 930 ± 9; 28 925	580 ± 52	268 ± 39	2.2 ± 1.1
		324 ± 32	272 ± 42	1.2 ± 0.75
acetyl TEM-1 β-lactamase	29 052 ± 7; 29 075[f]	682 ± 36	48 ± 11	14.0 ± 0.7
		g	*g*	*g*

[a] Reaction mixture consisted of 0.10 M sodium chloride buffered to pH 7.0 with 0.05 sodium cacodylate at 25 °C. Upper row values for kinetic parameters correspond to BENPEN; the lower row values correspond to SLPEN. [b] Determined by electrospray ionization mass spectrometry. Theoretical molecular weight is calculated according to the amino acid sequence (*33*, *34*) plus the chemical modification. [c] The steady-state kinetic parameters for cysteine mutants prepared in the absence of cacodylate buffer were equivalent to those reported here, confirming the absence of adduct formation of the free sulfhydryl group with arsenic(IV) (*35*, *36*). [d] Cysteine residue of mutant enzyme was chemically modified with MMTS. [e] Wild-type enzyme was reacted with acetylimidazole. [f] Calculated for reaction with four acetyl groups. Observed result corresponds to 3.55 ± 0.11 acetyl residues reacted per mole of wild-type TEM-1 β-lactamase. [g] Not determined for SLPEN.

to depress the freezing point of reaction mixtures, similar to the use of MeOH as cryosolvent for the class A staphylococcal PC1 β-lactamase (*37*) and β-lactamase I (*38*) enzymes. At ambient temperatures MeOH exhibited only noncompetitive inhibition of the TEM-1 enzyme up to concentrations of 50:50 MeOH:H_2O (v/v). The temperature dependence of k_{cat} and v_0/E_0 yielded an Arrhenius activation energy of 53.1 $\pm$ 1.5 kJ/mol, comparable to values of 47.3 and 51 kJ/mol reported for the *B. cereus* and *S. aureus* enzymes, respectively (*37*, *38*).

Although we have not been able to demonstrate kinetic separation for acylation and deacylation in cryoenzymologic experiments at temperatures above -50 °C, we have been able to demonstrate temporal resolution in the formation of the Michaelis complex and an acylenzyme reaction intermediate below -70 °C by difference absorption spectroscopy. The results are shown in Figure 3. Because changes in absorptivity associated with binding of SLPEN to the enzyme are too small for reliable quantification, we have employed the chromophoric substrate FAPEN. The values of the steady-state kinetic parameters $k_{cat} \approx 1760 \pm 19$ s^{-1} and $k_{cat}/K_M \approx 14.8 \pm 0.5 \times 10^6$ M^{-1} s^{-1} at pH 7 and 25 °C governing hydrolysis of FAPEN catalyzed by TEM-1 β-lactamase are equivalent to those of the nitroxyl spin-label probe. Also, FAPEN has been employed by Virden, Fink, and co-workers in cryokinetic studies of the PC1 β-lactamase and β-lactamase I (*37*, *38*). As evident in Figure 3, there is enhanced absorptivity of the chromophoric substrate in the near-ultraviolet region, allowing more accurate quantification of absorption changes induced through substrate binding.

In Figure 3 the spectral species labeled EY WT formed with wt TEM-1 β-lactamase was observed both at -35 °C and at -75 °C and was identified as the acylenzyme reaction intermediate because addition of the competitive inhibitor benzo[*b*]thiophene-2-boronic acid (*39*) with a K_i of $\sim 6 \times 10^{-6}$ M against the TEM-1 enzyme (A.S.-P. and M.W.M., unpublished observations) did not displace the chromophoric substrate from the wt enzyme or from the deacylation impaired Glu166Asn mutant. On the other hand, addition of the substrate to the enzyme at temperatures ≤ -70 °C was associated with immediate appearance of the spectral species labeled ES upon completion of mixing ($\sim$5 min under the high viscosity conditions of this cryosolvent mixture at this temperature). Addition of the inhibitor to sample and reference cuvettes immediately after appearance of the ES spectral species resulted in only a featureless baseline indicative of displacement of the substrate from the active site. Also, addition of the inhibitor prior to substrate prevented detectable formation of either spectral species. In the absence of the inhibitor at -75 °C, however, transformation of the ES spectral species into the EY species begins within approximately 10 min after mixing. As formation of the EY species increased, displacement of the chromophore from the enzyme by addition of inhibitor was correspondingly decreased.

The difference spectrum of the EY species in Figure 3 is distinguishable from the ES spectrum through the absence of the trough near 350 nm and the increased absorption intensity at 275 nm. Furthermore, the EY spectrum of the wt enzyme is essentially identical to the spectrum of the acylenzyme formed with the Glu166Asn mutant. Only at -70 °C or lower was detection of the noncovalent complex of the substrate bound to the enzyme feasible. In the -35 to

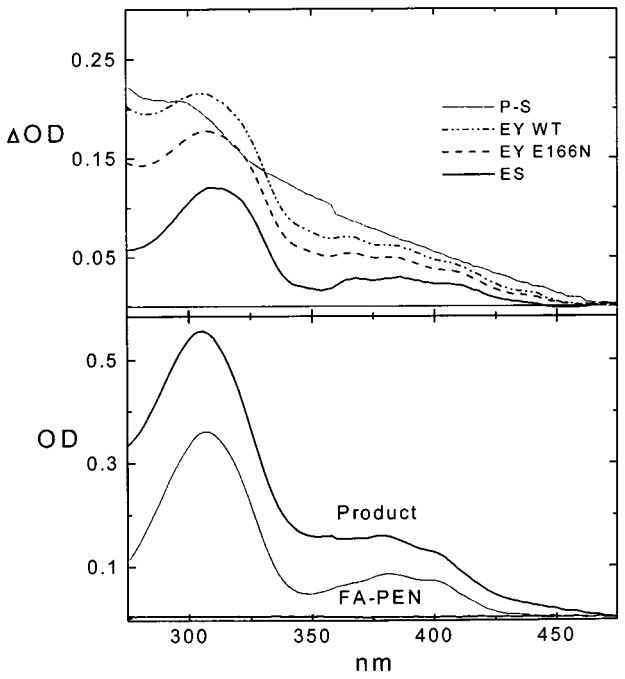

FIGURE 3: Difference absorption spectra of reaction intermediates of TEM-1 β-lactamase formed with the chromophoric substrate FAPEN. In the upper panel difference spectra are displayed from experiments using tandem cuvettes for a mixture of the enzyme with the substrate [in 70:30 (v:v) MeOH:H_2O cryosolvent containing 0.75 M NaCl buffered to pH 7.0 at -75 °C with 0.05 M cacodylate] minus the spectral contributions of the enzyme and substrate in the same cryosolvent mixture, each in a separate cuvette. The enzyme and substrate concentrations were 1.5×10^{-5} and 1.0×10^{-5} M, respectively. The lower panel illustrates the direct absorption spectra of the substrate and hydrolysis product in the same solvent at -20 °C obtained in a separate experiment. For the spectra in the lower panel, after collecting the spectrum of the substrate at a concentration of 1.0×10^{-5} M, enzyme (1×10^{-6} M) was added to both sample and reference cuvettes to collect the direct absorption spectrum of the product. A small artifact is seen in the spectrum at 360 nm in the (P$-$S) difference spectrum due to conversion of the tungsten light source in the spectrophotometer to a deuterium lamp. The product-minus-substrate (P$-$S) difference spectrum in the upper panel is calculated from the direct absorption spectra in the lower panel. The following conditions apply: EY WT, formation of the spectral species designated as the wt acylenzyme because the absorption due to the chromophoric FAPEN substrate could not be displaced by addition of the benzo[*b*]thiophene-2-boronic acid inhibitor; EY E166N, the same as for the wt enzyme except applied to the Glu166Asn mutant; ES, spectral species formed immediately upon mixing and designated as the Michaelis complex because the absorption due to the FAPEN substrate could be annihilated by addition of benzo[*b*]thiophene-2-boronic acid. Formation of the ES species was observed only prior to formation of the EY WT species. See text for further discussion.

-50 °C temperature range only the acylenzyme species was observed because the noncovalent species was not sufficiently long-lived. We have also observed comparable spectral changes in the -60 to -85 °C temperature range with use of BENPEN and β-lactamase I of *B. cereus*, adding borate as the inhibitor to separate formation of the acylenzyme from the Michaelis complex (D.M. and M.W.M., unpublished observations). However, the spectral changes are of lower amplitude than those described here for the furanyl-propenoyl chromophore. Also, the influence of borate as an inhibitor (*40*) is much weaker than that of the benzo[*b*]thiophene-2-boronic acid inhibitor employed here. The

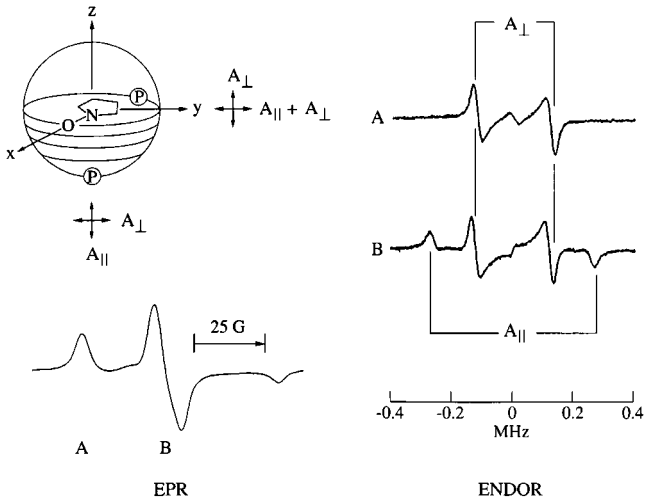

FIGURE 4: Magnetic interactions governing angle-selected ENDOR of a nitroxyl spin-label. In the upper, left-hand diagram, are shown the relationships of the molecular axes to the principal axes of the $\boldsymbol{g}_e$ tensor of the nitroxyl group and the *A* tensors of nearby protons. Relative positions of protons in the *x,y* plane or on the *z* axis are also indicated. In the lower left-hand portion, a frozen solution EPR spectrum of a spin-label is shown. Setting A is defined by $\mathbf{H}_0$ set to the low-field spectral feature while setting B is defined by $\mathbf{H}_0$ set to the central EPR spectral feature. Two ENDOR spectra are shown which would correspond to spectra of a spin-labeled penicillin totally deuterated at all positions except at H(6). The abscissa measures the observed ENDOR shift $\Delta\nu = \nu_{ENDOR} - \nu_H$ where ν_{ENDOR} represents the observed frequency and ν_H represents the proton Larmor frequency.

results, nonetheless, confirmed that an acylenzyme accumulates with BENPEN as the substrate and that the observations in Figure 3 are not limited to use of only FAPEN. We also compared the stability of formation of the acylenzyme reaction intermediate with FAPEN in the low temperature range at pH 5 and 9. The difference absorption changes were less pronounced and more difficult to quantify; consequently our experiments were all carried out at pH 7. In general, these results are comparable to those obtained in our earlier optical studies of carboxypeptidase A in which the reaction was shown to proceed via the sequential formation of a Michaelis complex and a mixed anhydride (acylenzyme) intermediate with rate-limiting breakdown of the acylenzyme (*8*, *22*, *41*).

ENDOR Characterization of the Acylenzyme of TEM-1 β-Lactamase

A Brief Summary of the Principles of Angle-Selected ENDOR of Nitroxyl Spin-Labels. Detailed descriptions of the physical basis of angle-selected ENDOR of spin-labels are found in earlier publications (*9*, *10*). For a spin-label immobilized in a polycrystalline state or in frozen glassy solutions, as in this investigation, Figure 4 illustrates the basic geometrical relationships underlying the orientation dependence of hf couplings of nearby protons with the unpaired electron of the nitroxyl group as a function of the static (laboratory) magnetic field $\mathbf{H}_0$. The hf interactions are governed by the $\boldsymbol{g}_e$ tensor, which defines the principal axes of the interactions of the unpaired electron, and the $\boldsymbol{A}$ tensor, which correspondingly describes the principal hyperfine axes of a proton. In spin-labels, the axes of the $\boldsymbol{g}_e$ and $\boldsymbol{A}$ tensors are essentially coincident and *g* anisotropy is very small. The g_z component of $\boldsymbol{g}_e$ is coincident with the molecular *z* axis and, therefore, perpendicular to the molecular *x,y* plane. In Figure 4 the low-field absorption feature of the EPR spectrum arises from those molecules for which the g_z component is coincident with the static magnetic field $\mathbf{H}_0$. Microwave power saturation that drives the transitions of the unpaired electron then selects perpendicularly oriented molecules for monitoring nuclear resonance transitions with resultant "single-crystal-like spectra" (*42*). We have termed this condition *setting A*. On the other hand, microwave saturation of the intense central feature of the EPR spectrum selects molecules of all orientations. This is termed *setting B*.

As illustrated in Figure 4 for setting A, a proton in the plane of the spin-label gives rise to the perpendicular hf interaction $A_\perp$ while a proton located on or near the molecular *z*-axis gives rise to the parallel hf interaction $A_\parallel$. On the other hand, for setting B of the laboratory magnetic field, an axially located proton gives rise to a perpendicular interaction $A_\perp$ while a proton in the molecular plane gives rise to both parallel ($A_\parallel$) and perpendicular ($A_\perp$) interactions. This differential appearance of parallel and perpendicular hf couplings dependent on orientation of the spin-label with respect to the (static) laboratory magnetic field $\mathbf{H}_0$ provides a diagnostic signature for assigning the relative position of the detected magnetic nucleus according to the axes of the $\boldsymbol{g}_e$ tensor (*9*, *10*). In addition, of critical diagnostic importance is that the ENDOR splitting for the perpendicular hf interaction $A_\perp$ is to first-order independent of the setting of the magnetic field $\mathbf{H}_0$ while the ENDOR splitting for the parallel interaction $A_\parallel$ varies and passes through a maximum value when $\mathbf{H}_0$ reaches the canonical orientation corresponding to the principal hfc component (*43*, *44*). In the description of ENDOR spectra of the spin-labeled acylenzyme reaction intermediate, assignment of resonance features based on these physical relationships was confirmed in each case through experiment.

By measuring the energy of the electron-nucleus hf interaction *A*, the separation between the unpaired electron of the nitroxyl group (*45*) and each ENDOR-active nucleus can be estimated according to eq 1.

$$A = \frac{g_N|\beta_N|g_e|\beta_e|}{hr^3}(3\cos^2\alpha - 1) + A_{iso} \qquad (1)$$

In this relationship, the *g*'s represent the electron and nuclear *g* factors; the *β*'s represent the electron and nuclear Bohr magneton, respectively; *h* is the Planck constant; *r* is the electron-nucleus distance; α represents the angle between the static magnetic field $\mathbf{H}_0$ and the electron-nucleus position vector $\mathbf{r}$; and A_{iso} is to first-order the isotropic hfc due to the Fermi contact interaction.

For the resonance conditions illustrated in Figure 4 according to eq 1, the observed ENDOR shifts correspond to the principal hfc components $A_\parallel$ and $A_\perp$ with values of the dipolar angle α of 0° for parallel hf interactions and 90° for perpendicular hf interactions, respectively. Since the value of A_{iso} can be estimated according to the constraint $(A_\parallel + 2A_\perp) = 3A_{iso}$, the dipolar hfc components $A_\parallel^D$ and $A_\perp^D$ representing the first right-hand term of Equation 1 are then obtained by subtracting A_{iso} from the observed values of $A_\parallel$ and $A_\perp$. In this manner the electron-nucleus separation *r* can be estimated directly from the hf couplings identified in the spectrum.

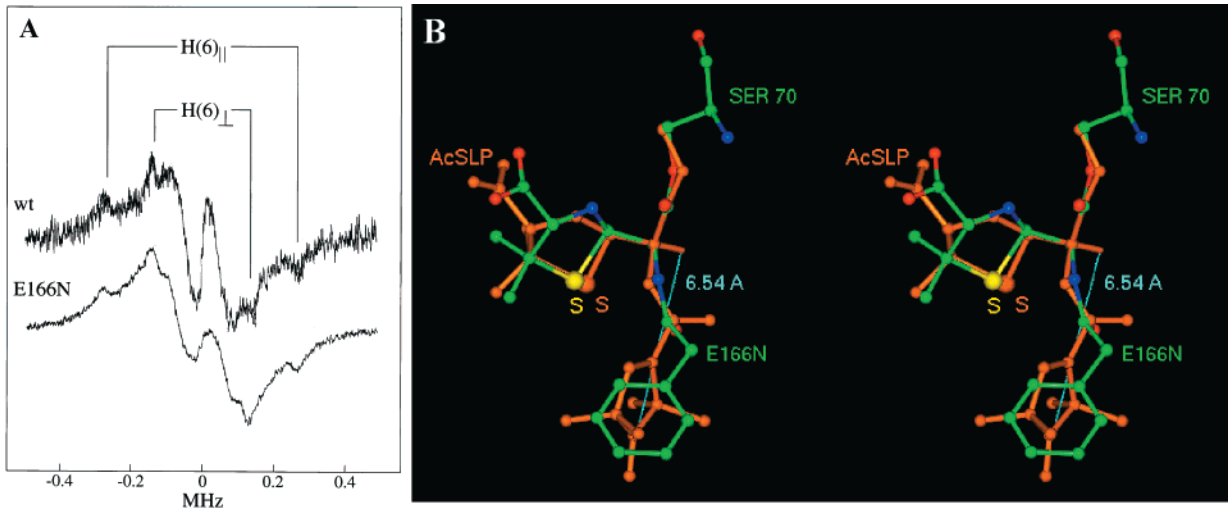

FIGURE 5: (A, left) Proton ENDOR spectra of the reaction intermediate of wt TEM-1 β-lactamase and of the Glu166Asn mutant formed with SLPEN under conditions of enzyme in excess. The wt enzyme and Glu166Asn mutant were biosynthetically enriched with deuterium (88−90% ^{2}H). The spectra were recorded with $\mathbf{H}_0$ at setting B. The stick diagrams indicate the parallel and perpendicular hfc components of H(6) of the spin-labeled acyl moiety. Enzyme and substrate concentrations were 5.7×10^{-4} and 4.5×10^{-4} M, respectively, in a [^{2}H$_4$]methanol:^{2}H$_2$O (40:60 v/v) cosolvent mixture containing 1 M NaCl buffered to pD 7.5 with 0.04 M sodium cacodylate. For the Glu166Asn mutant an identical spectrum was obtained by reaction of the mutant and substrate at room temperature. The abscissa shows the ENDOR shift as defined in Figure 4. (B, right) Stereo diagram shows the ENDOR assigned conformation of the spin-labeled penicilloyl-serine-70 moiety in the acylenzyme of the wt protein (labeled AcSLP with orange-yellow rendering) superpositioned onto the X-ray defined benzylpenicilloyl-serine-70 moiety of the acylenzyme of the Glu166Asn mutant. The latter is rendered with standard coloring of green (C), red (O), blue (N), and yellow (S) for each chemical element.

The effective dipolar position of the unpaired electron spin associated with the nitroxyl group lies approximately at the midpoint of the N−O bond and is defined to within ±0.04 Å (*9*, *45*). By application of ENDOR we have shown that dipolar electron-nucleus distances can be determined over a 4−10 Å range with errors no greater than 5% based on ENDOR line width (*7*−*12*, *44*−*46*). This precision of structural analysis is greater than that achieved by other physical methods for molecules in solution and in fact is exceeded only by that of single-crystal X-ray diffraction. For nuclei for which $r \geq 5$ Å, the isotropic contributions are negligibly small. We can then use the observed hfc components directly to estimate electron-nucleus distances. The validity of this approximation has been demonstrated in numerous ENDOR studies of spin-labeled compounds, including spin-labeled penicillin and cephalosporin (*7*−*12*, *44*−*47*).

Characterization of the Acylenzyme Reaction Intermediate of TEM-1 β-Lactamase by ENDOR Spectroscopy. Because the steady-state kinetic parameters of the furanyl-propenoyl substrate are comparable to those of SLPEN, we have applied cryosolvent conditions based on the results in Figures 3 to characterize the acylenzyme reaction intermediate by ENDOR spectroscopy. Figure 5A illustrates proton ENDOR spectra of the Glu166Asn mutant and of wt TEM-1 β-lactamase reacted with SLPEN in a cryosolvent mixture at −35 °C. To detect resonance absorptions of discrete classes of hydrogens, as seen in Figure 5A, modulation conditions are of paramount importance. Under conditions of high modulation amplitude, e.g., 50−100 kHz amplitude modulation of the rf field, only diffuse, unstructured resonance absorption is observed that is centered at the Larmor frequency and is known as matrix ENDOR (*48*). Under the conditions of high modulation amplitude necessary to observe matrix ENDOR, the resonance features of nearby hydrogens of diagnostic and structural interest that are of much smaller line width are overmodulated and are not distinguishable from matrix ENDOR. Therefore, to detect the resonance absorption of discrete classes of nearby hydrogens that are not randomly distributed with respect to the paramagnetic probe, low amplitude modulation of the rf field (≤12 kHz) must be applied (*7*−*12*, *44*−*47*; cf., Methods and Materials). These conditions deemphasize the resonance absorption of hydrogens contributing to matrix ENDOR.

In Figure 5A, the small fraction of distant, randomly distributed, covalent hydrogens remaining in the protein under conditions of high deuterium enrichment contribute only to matrix ENDOR which remains weak because of the low (amplitude) modulation conditions used. On the other hand, resonance features that arise from nearby hydrogens of structural importance can be observed "on top" of the broad matrix ENDOR line because of low modulation amplitude of the rf field. As illustrated in Figure 5A, two pairs of resonance features are observed. As the closest ENDOR-active nucleus to the nitroxyl probe on the substrate, H(6) (cf., Figure 1B for atomic numbering scheme of SLPEN) is the only nucleus associated with sufficient peak-to-peak amplitude to be detected under these modulation conditions (*11*, *12*). Thus, the resonance features in Figure 5A are ascribed to its principal $A_{||}$ and $A_{\perp}$ hfc components on the basis of $\mathbf{H}_0$ settings. Observation of the same hf splitting for the wt enzyme as for the deacylation impaired Glu166Asn mutant confirms that the spectrum of the wt enzyme corresponds to an acylenzyme reaction intermediate with the same conformation of the spin-labeled acyl moiety. The ENDOR splittings identical in both wt and mutant species yield an electron−H(6) distance of 6.54 ± 0.10 Å. These resonance features and their corresponding electron-nucleus distance are distinguishably different from that for the free product of the reaction (*12*). In Table 2, we have summarized values of the observed hfc components and the electron-nucleus distance *r* calculated for H(6). Results for

Table 2: Summary of hfc Components and Estimated Dipolar Electron−Proton Distances in the Spin-labeled Penicilloyl Acylenzyme Reaction Intermediate of TEM-1 β-lactamase

proton	$A_{\|\|}$ (MHz)	$A_{\perp}$ (MHz)	r (Å)[a]
H(6) (SLPEN)	0.57	0.29	6.54 ± 0.10
CH_3 (acetyl-Tyr105)	0.38	0.20	7.49 ± 0.15[b,c]
CH_3 (Glu240Cys-SCH_3)		0.28	6.57 ± 0.15[c]
CH_3 (Met272Cys-SCH_3)	0.475	0.242	6.91 ± 0.10[c]
H′ (solvent water molecule)	0.54		6.65 ± 0.10
H″ (exchangeable proton)	0.90		5.61 ± 0.10

[a] We have previously shown (*9*, *10*) for nitroxyl spin-labels that the dipolar hfc components $A_{\|\|}^D$ and $A_{\perp}^D$ can be calculated under the constraint $(A_{\|\|} + 2A_{\perp}) = 3A_{iso}$, where $A_{\|\|}$ and $A_{\perp}$ are the observed ENDOR splittings for the principal parallel and perpendicular hfc components, respectively. We have also demonstrated through ENDOR and TRIPLE spectroscopy that $A_{\|\|} > 0 > A_{\perp}$ for nitroxyl spin-labels (*9*, *47*). Since the isotropic contributions of distant protons (≥5 Å) are vanishingly small, we have calculated values of r for three classes of protons on the basis of only one observed principal hfc component. Uncertainty in the ENDOR shift of 15−20 kHz estimated from the line width of ENDOR absorptions is included as the uncertainty in the calculation of electron−proton distances. [b] The separations of O^{ξ} for the other three tyrosine residues (tyrosine-264, 17 Å; tyrosine-97, 19 Å; tyrosine-46, 26 Å) from the nitroxyl group render them too distant for spectroscopic detection. [c] Since the methyl hydrogens are not spectrally resolved at these electron-nucleus distances under the modulation conditions employed (*9*, *49*), the distance to the geometrically averaged proton only is estimated.

other classes of protons that are discussed below are also given.

Figure 5B illustrates the acyl moiety of the spin-labeled penicillin substrate constructed into the active site of TEM-1 β-lactamase constrained by the ENDOR determined electron-H(6) distance of 6.54 ± 0.10 Å and the van der Waals hard sphere limits of substrate and active-site atoms. This is compared to the benzylpenicilloyl group of the Glu166Asn mutant acylenzyme refined at 1.7 Å resolution (*14*; N. C. J. Strynadka and M. N. G. James, personal communication). For this graphics comparison, the only non-ENDOR structural constraints for the wt enzyme invoked were van der Waals hard sphere limits of nonbonded atoms and attachment of the acyl moiety of SLPEN to O^{γ} of serine-70 according to typical bond distance and valence angle parameters of an ester linkage (cf., Methods and Materials). As seen in the stereo diagram, there is virtually complete overlap of the two structures except for the slightly different orientation of the benzyl group in the X-ray structure. This part of the active site does not place tight steric restrictions on orientation of the 6-*N*-acylamido group of the β-lactam substrate. Because of hard-sphere constraints defined by active-site residues and the structural requirements of the ester bond between the acyl moiety of the substrate and the side chain of serine-70, the single spectroscopically determined electron-nucleus distance of 6.54 ± 0.10 Å is sufficient to define the conformation of the spin-labeled penicilloyl moiety in the active site.

Figure 6 illustrates ENDOR spectra of chemically modified amino acid side chains that serve as probes of active-site structure. The resonance feature identified by an arrow in the upper set of spectra is assigned to the CH_3- group of acetyl-tyrosine-105 through its disappearance upon reaction of the enzyme with [$^2H_3$]acetylimidazole (the next nearest tyrosinyl residue is ≥17 Å, rendering it undetectable). The

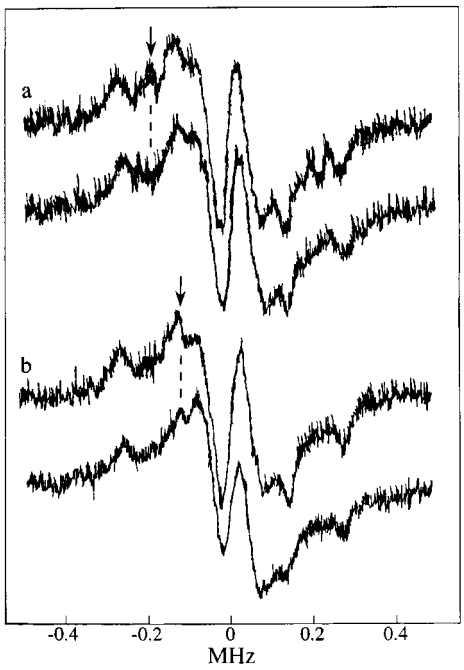

FIGURE 6: Comparison of proton ENDOR spectra of spin-labeled acylenzyme reaction intermediates formed with acetylated wt TEM-1 β-lactamase (upper set of spectra, labeled **a**) and with the Glu240Cys mutant in which the cysteine-240 side chain has been modified with MMTS (lower set of spectra, labeled **b**). In each case, enzyme biosynthetically enriched with deuterium (88−90% ^2H) was used. The spectrum for each acylenzyme intermediate reacted with acetylimidazole, correspondingly, MMTS (top spectrum in each set) is compared to the spectrum obtained for the enzyme reacted with [$^2H_3$]acetylimidazole, or [$^2H_3$]MMTS (bottom spectrum in each set). The resonance feature specific for each chemically modified side chain, highlighted by an arrow, is absent in the spectrum of the deuterated analogue. In the lower set of spectra it is evident that a small resonance feature overlapping with that for the thiomethoxy group remains after reaction with [$^2H_3$]-MMTS. Since the ENDOR shift for this feature is precisely identical to that for the $A_{\perp}$ feature of H(6) in Figure 5 we conclude that this weak feature represents the overlapping contribution of H(6) in the substrate. Other conditions as in Figure 5.

lower set of spectra in Figure 6 belongs to the Glu240Cys mutant in which the mutant cysteinyl side chain has an attached CH_3S- group through reaction with MMTS. The decrease in intensity for the deuterated analogue similarly identifies the resonance feature belonging to the CH_3S-group. Comparable results were obtained for the acylenzyme of the Met272Cys mutant (spectra not shown), and the corresponding electron-nucleus distance is listed in Table 2.

Figure 7 illustrates the structural relationships of the spin-labeled penicilloyl moiety in the active site of TEM-1 β-lactamase to the three side chains of active-site residues that have been chemically modified to serve as ENDOR probes. In this diagram, the conformation of the spin-labeled acyl moiety is identical to that in Figure 5B. For graphics interpretation of the ENDOR structural results, we applied the preferred rotamer conformations (*51*) of amino acid residues to model the side chains of tyrosine-104, cysteine-240, and methionine-272. The conformations of the chemically modified side chains for residues tyrosine-105 and methionine-272 required little adjustment and are nearly identical to their unmodified counterparts in native TEM-1 β-lactamase (*30*). On the other hand, the thiomethoxy-modified side chain of cysteine-240, as seen in Figure 7, is

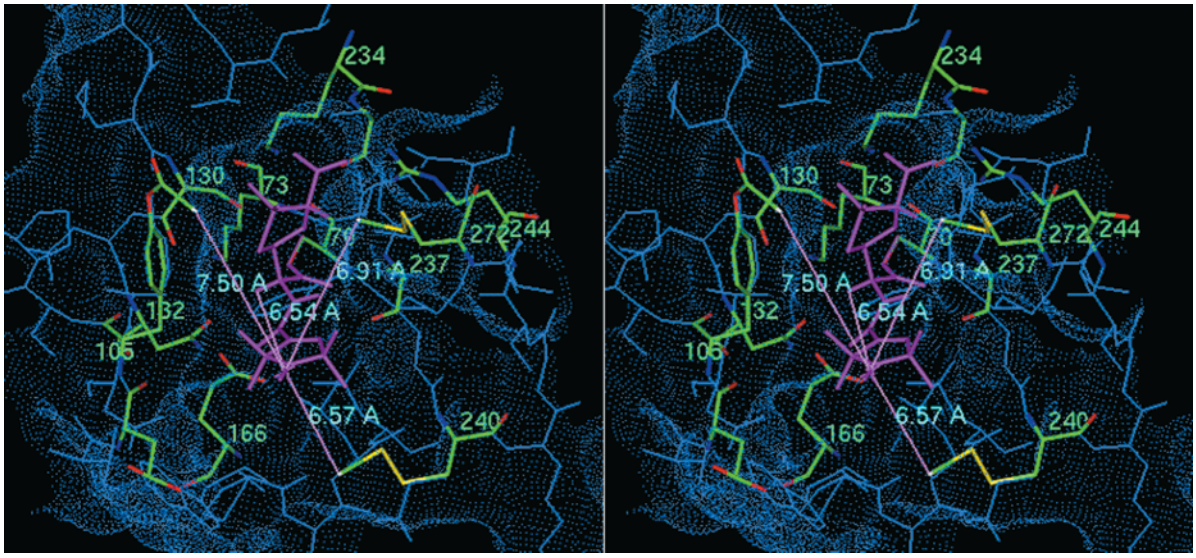

FIGURE 7: Stereoview of the active site of the acylenzyme of TEM-1 β-lactamase formed with SLPEN. The conformation of the substrate is constrained, as in Figure 5B, by the ENDOR determined electron−H(6) distance in the spin-labeled penicilloyl moiety indicated in cyan color. ENDOR determined electron−proton distances from the unpaired electron of the nitroxyl group (*45*) to the methyl group of acetyl-tyrosine-105 (7.49 Å) and to the thiomethoxy groups attached to the mutant cysteinyl side chains of Glu240Cys (6.57 Å) and Met272Cys (6.91 Å) are also indicated. The blue dotted surface represents the calculated solvent accessible surface of the active site (*50*). The acetyl group attached to the side chain of tyrosine-105 has been constructed according to the X-ray defined structure of 2-acetoxy-3-methyl-benzoic acid (*31*) while the thiomethoxy group attached to the −SH group of mutant cysteinyl residues has been modeled according to the structure of 2-desamino-L-cystine (*32*).

slightly shifted from the X-ray defined position of the corresponding glutamate residue in the wt enzyme. The steric constraints of active-site residues allow virtually no additional degrees of freedom to accommodate the substrate in its catalytically competent conformation.

ENDOR Detection of the Hydrolytic Water Responsible for Acylenzyme Breakdown. In Figure 8, we have compared ENDOR spectra of deuterium enriched spin-labeled reaction intermediates of the wt and E166N enzymes in protiated solvent. In Figures 5 and 6 proton resonances specific for the substrate and chemically modified side chains could be detected only against the background of deuterium enriched protein in perdeuterated solvent. Consequently, the large number of protons contributing to the spectra in Figure 8 obliterates the resonance features of the substrate. There is broad underlying resonance absorption due to the presence of exchangeable protons in the enzyme and protiated solvent. Two resonance features are identified above this broad background resonance absorption that cannot be attributed to bulk solvent. These features, labeled H′ and H″, therefore, must arise from solvent exchangeable protons of amino acid residues or solvent molecules sequestered in the protein. In the upper panel of Figure 8, it is seen that the feature labeled H″ has the same shape and occurs at precisely the same resonance position for both the wt enzyme and the Glu166Asn mutant. On the other hand, the expanded scale in the upper panel of Figure 8 shows that the feature labeled H′ is distinct for the wt enzyme. The maximum for feature H′ is measurably shifted from the position of maximum intensity for the mutant and occurs at a resonance frequency where there is only decreasing, structureless intensity in the mutant spectrum.

The resonance features H′ and H″ are assigned to parallel hfc components on the basis of angle-selected ENDOR as described above. The ENDOR splitting for the resonance feature labeled H″ in Figure 8 yields an electron-to-nucleus distance of 5.61 ± 0.10 Å while that for H′ corresponds to a distance of 6.54 ± 0.10 Å. As illustrated in the upper part of Figure 8, we identified the origin of the H″ resonance common to both wt and Glu166Asn mutant enzymes by examining which active-site residues have exchangeable protons coinciding with the surface of a sphere of 5.61 Å radius centered on the electronic point dipole of the nitroxyl group. The only residue that could account for the resonance was the $-NH_2$ group of asparagine-132 which lies close to the surface of the sphere and almost exactly in the plane of the oxypyrrolinyl ring,[2] as required by the pattern of ENDOR features in Figure 8. On the other hand, since the H′ feature corresponding to a 6.65 Å distance is not observed for the Glu166Asn acylenzyme, the resonance must arise in a region of the wt enzyme that differs structurally. This difference, therefore, is likely to involve the immediate environment of the side chain of glutamate-166. Since no other structural difference between the wt and Glu166Asn enzymes can be identified, we attribute the H′ resonance feature to sequestered water in the immediate vicinity of the carboxylate group of glutamate-166.

To identify the location of the sequestered water molecule, we searched for possible hydrogen-bonding contacts that could stabilize a sequestered water molecule within van der Waals hard-sphere constraints. The electron−proton distance of 6.65 ± 0.10 Å was best accounted for by a hydrogen of a water molecule lying close to the molecular plane of the spin-label and hydrogen bonded to the $O^{\epsilon 1,2}$ atoms of the side chain of glutamate-166, as illustrated in the lower part

[2] Because of intrinsic line widths, the two hydrogens of the carboxamide side chain of asparagine-132 are not resolvable for an electron-nucleus separation of ~5.6 Å under the modulation conditions employed (*9*, *49*).

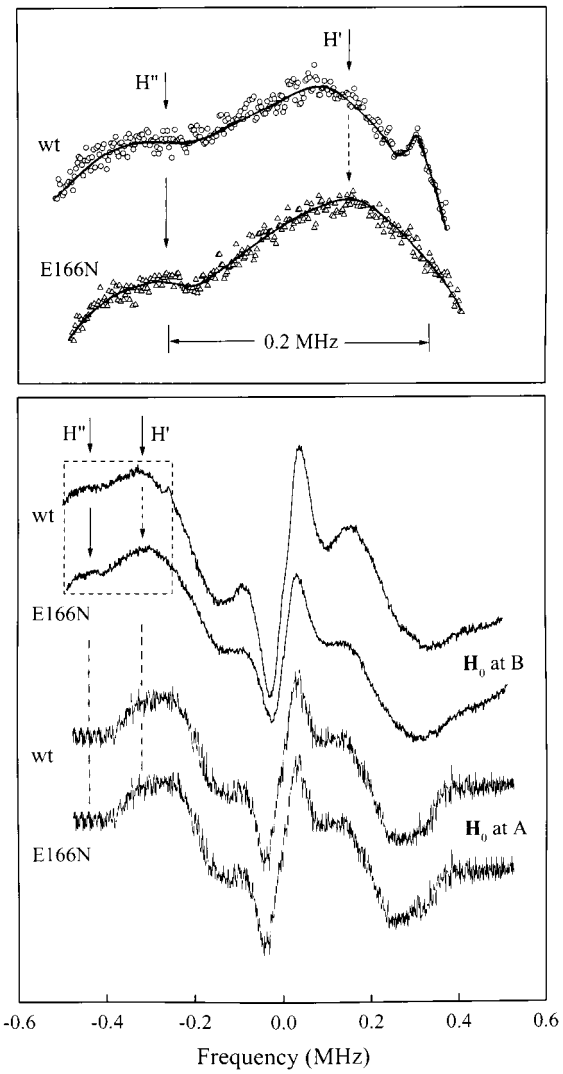

FIGURE 8: Comparison of proton ENDOR spectra of the acylenzyme intermediate formed with SLPEN and deuterium enriched wt enzyme and with deuterium enriched Glu166Asn mutant enzyme in protiated cryosolvent buffer. Pairs of spectra labeled for wt and mutant (E166N) enzyme are shown for A and B settings of $\mathbf{H}_0$ as lower and upper sets, respectively, in the lower panel. Two line pairs observed only in the B setting spectra of the wt and Glu166Asn mutant species are indicated by arrows labeled H′ and H″, respectively, and are also illustrated at higher gain in the upper panel. Comparison of their respective line shapes and positions shows that the feature associated with the larger splitting, labeled H″, is present in spectra of both the wt and Glu166Asn mutant enzyme for $\mathbf{H}_0$ at B, while the feature associated with the smaller splitting, labeled H′, is seen only for the wt enzyme. The solvent was 40:60 (v/v) [$^2H_3$]methanol: H_2O buffered to pH 7.0 with 0.02 M cacodylate. Other conditions are as indicated in Figure 5A.

of Figure 9. The ENDOR-defined water molecule sits just on the extended van der Waals surface (*50*) of the substrate. The water oxygen lies at an approximate 2.9 Å distance from the C(7) atom of the scissile ester bond and forms an angle of ∼105° with the C(7)−O(8) bond vector, precisely that expected for O···C═O nucleophilic attack (*52*). There was no other identifiable site that could sterically accommodate a solvent molecule at the ENDOR required distance and provide hydrogen bonding for stabilization. Furthermore, the side chain of lysine-73 could not be torsionally altered so as to allow hydrogen bonding with a solvent molecule compatible with the ENDOR data.

To confirm our assignment of a sequestered water molecule to account for the resonance feature H′ observed only for the wt acylenzyme, we have also carried out spectral simulations, adding the first-derivative resonance features anticipated for a water proton, positioned as illustrated in Figure 9, to the observed spectrum of the Glu166Asn acylenzyme (E. V. Galtseva and M.W.M., unpublished observations). As expected according to angle-selected principles outlined above and applied to Figure 8, the parallel hf coupling feature of the proton adds to the spectrum of the mutant at the position indicated by the arrow for H′ while the peak-to-peak amplitude of the perpendicular hf coupling feature closer to the Larmor frequency is greatly diminished by the decreasing broad, structureless intensity observed in this frequency region in the mutant spectrum. Interestingly, the perpendicular hf coupling feature of the second proton of the water molecule, modeled according to idealized geometry at a distance of 8.1 Å, provides an explanation for the deeper trough near the matrix ENDOR signal observed for the wt enzyme while its parallel hf feature is obliterated through overlap with the perpendicular feature of the first proton and the decreasing broad intensity observed for the mutant. The small sharp feature observed in the wt spectrum with a smaller ENDOR shift is best accounted for as a summation effect, resulting from addition of the parallel hf coupling contribution of the water proton to the mutant spectrum to the left of its maximum intensity. Because no rigorous theory has been developed to account for intensity of ENDOR absorptions of disordered solids and the relative intensity of features from different classes of protons is expected to be sensitive to distance, orientation, and anisotropy of relaxation (*53*), further conclusions at present cannot be drawn through spectral simulations. Nonetheless, the observed differences in the wt and mutant spectra around H′ are reasonably accounted for by anticipated contributions of a water molecule modeled as illustrated in Figure 9.

Chemical Role of Glutamate-166 in TEM-1 β-Lactamase

In the catalytic action of TEM-1 β-lactamase, two processes require the participation of a general base. One is activation of the O−H group of serine-70 through proton abstraction for nucleophilic attack on the β-lactam carbonyl carbon atom. The other is activation of a water molecule for breakdown of the acylenzyme. Hitherto, it has not been directly established whether two separate residues serve as general base catalysts in the reaction or whether one residue facilitates both processes. Strynadka and co-workers postulate that the side chain of lysine-73 promotes proton abstraction as a general base catalyst (*14*, *54*). This suggestion implicitly assigns the pK_a of ∼4.4 governing the acidic limb of the pH profile of k_{cat} to lysine-73 (cf., Figure 2). In direct contradiction to this suggestion, Damblon and co-workers have shown by NMR titrations of catalytically active TEM-1 β-lactamase biosynthetically enriched with [ε-^{13}C]lysine that the pK_a of lysine-73 is ≥10 (*55*). By estimating the electrostatic contributions to the free energy changes associated with acylenzyme formation in TEM-1 β-lactamase, we have recently shown that abstraction of the proton from the O−H group of serine-70 is energetically more favorable when catalyzed by a water molecule hydrogen bonded to the carboxylate side chain of glutamate-166 than by the bare carboxylate group or a neutral amine form of lysine-73 (*17*).

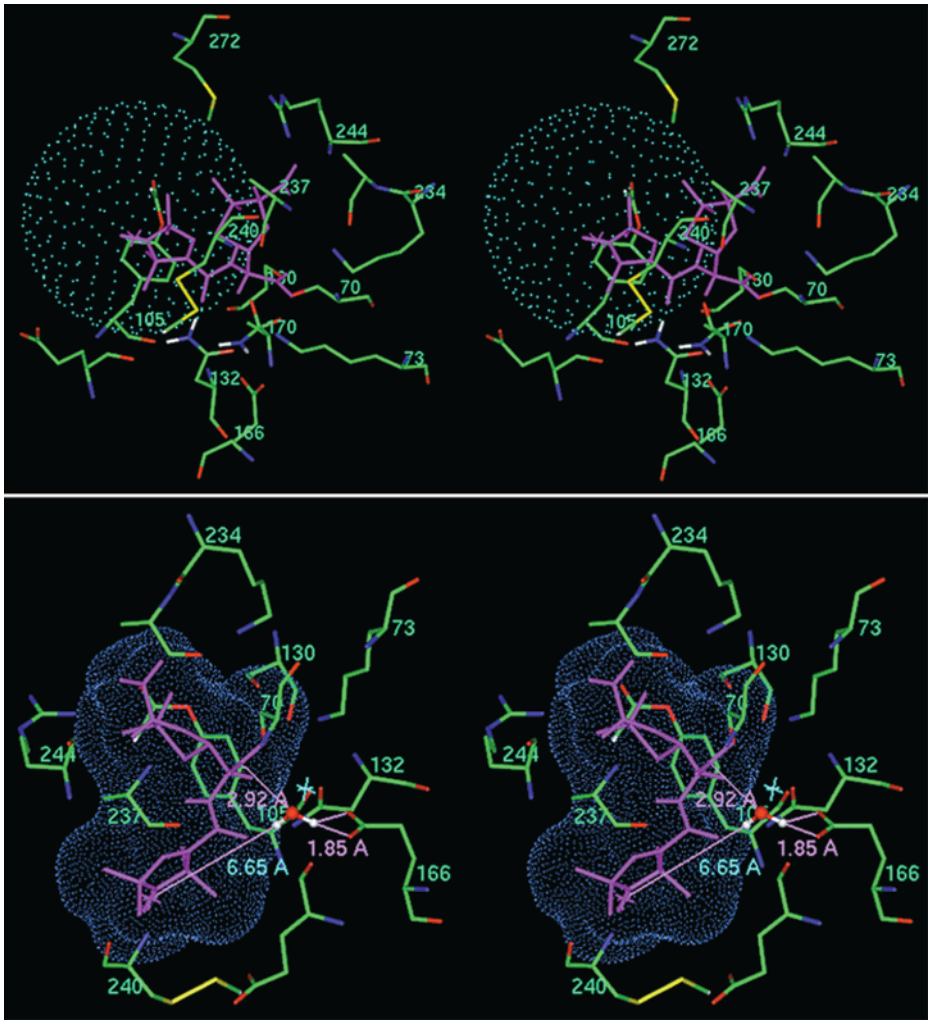

FIGURE 9: Stereo diagrams illustrating identification of the location of the H′ and H″ protons by molecular graphics. In the upper stereo diagram a sphere of 5.61 Å radius corresponding to the H″ hfc component is centered on the effective dipolar position of the spin-label nitroxyl group (*45*) in its ENDOR constrained conformation, as defined in Figure 5. The lower stereo diagram shows the location of the ENDOR-identified water molecule (giving rise to the H′ resonance feature) sequestered in the active site (colored red with white hydrogens). The ENDOR determined distance from the unpaired electron to the water proton is colored cyan while structural relationships to the carboxylate oxygens of glutamate-166 and to C(7) of SLPEN derived from modeling are shown in magenta. The dotted surface represents the extended van der Waals surface (*50*) of the spin-labeled acyl moiety showing that the water molecule is just accommodated sterically by the substrate. The star just above the ENDOR-defined water molecule indicates the position of an X-ray-defined water molecule in the free enzyme (*30*).

Hitherto, structural evidence implicating glutamate-166 as catalytically required in the reaction mechanism of class A β-lactamases has come from the observations that substitution of the glutamate residue with a neutral amino acid such as glutamine or asparagine renders the enzyme deacylation impaired (*13*, *14*). Similarly, the Asn170Gln mutant of PC1 β-lactamase is deacylation impaired because the longer side chain of a glutamine residue at position 170 sterically prevents a water molecule from hydrogen bonding to glutamate-166 (*56*). Thus, while the results of these crystallographic studies support the notion that the side chain of glutamate-166 functions as the general base catalyst for breakdown of the acylenzyme intermediate, direct detection of the hydrogen-bonded water molecule in the wt enzyme has not been feasible because at room temperature the reaction intermediate is too labile for crystallographic identification. On this basis ENDOR detection of a water molecule sequestered within hydrogen-bonding distance to the $-COO^-$ group of glutamate-166 in the active site of the acylenzyme trapped through cryokinetic isolation, as shown through Figures 8 and 9, provides *direct* structural characterization of the functional role of this residue as the general base catalyst activating the hydrolytic water molecule. In fact, this is the only instance in which the catalytic role of an active-site residue activating a hydrogen-bonded water molecule as the nucleophile has been directly demonstrated in the active site of a *catalytically competent* enzyme reaction intermediate. For all other enzymes the role of a hydrogen-bonded water molecule as a nucleophile in the catalytic mechanism has been invoked only through indirect argument, as in the case of the Glu166Asn mutant (*14*) or the Asn170Gln mutant of the PC1 enzyme (*56*).

Since the ϵ-amine group of lysine-73 in the acylenzyme intermediate is more than 4 Å distant from the ENDOR detected water molecule, as illustrated in Figure 9, hydrogen bonding to the ENDOR water is not energetically favored. There are, however, interesting structural relationships between the side chain of lysine-73, the carboxylate group of glutamate-166, and the X-ray defined water molecule as observed in the free enzyme (cf., Figure 9) that suggest a

possible route through which the ENDOR detected hydrolytic water becomes activated as a nucleophile. In Figure 9 the water molecule identified by X-ray in the free enzyme (*30*) is located only 1.4 Å from the site where the ENDOR-active water becomes sequestered upon acylenzyme formation. While lysine-73 cannot enter into hydrogen-bonding relationships with the ENDOR-water, the X-ray defined water in the free enzyme readily forms a hydrogen-bonding bridge between the carboxylate group of glutamate-166 and the charged ϵ-amine group of lysine-73. In this hydrogen-bonded complex, the two charged side chains could be viewed as keeping the water molecule positioned to begin its transformation into a nucleophile. After substrate binding with formation of the acylenzyme intermediate, the hydrogen-bonded water−carboxylate complex shifts to begin nucleophilic attack as lysine-73 moves away from the X-ray defined water molecule, allowing the water molecule to occupy its ENDOR defined position. The negative charge on the side chain of glutamate-166 becomes consequently increasingly less compensated electrostatically as lysine-73 moves away. To adjust to this change in electrostatic environment, polarization of an H−O bond in the water molecule must become more pronounced, resulting in formation of a $\text{-COO}^{-}\cdots\text{H}^{\delta+}\text{-OH}^{\delta-}$ species. As the charge on the water hydrogen increases to form a discrete proton to neutralize the negative charge on the carboxylate group, the resultant increasing negative charge on the OH portion of the water molecule potentiates its nucleophilicity for breakdown of the acylenzyme reaction intermediate. The location of the ENDOR detected water, as identified through Figures 8 and 9, is likely the closest noncovalent position to the carbonyl carbon that the water molecule can occupy to begin formation of a tetrahedral adduct and hydrolytic bond cleavage.

It is of interest to note that a sequestered water molecule was not detected by ENDOR for the Glu166Asn mutant. This result is consistent either with disordered solvent or with the absence of structured water in the active site. The rate constant for acylation in the Glu166Asn mutant compared to that for the wt enzyme is decreased by a factor of $\sim 10^{-3}$ in contrast to the decrease of $\sim 10^{-8}$ for deacylation (*57*). Although glutamate-166 is not present to participate as a general base for acylation in the Glu166Asn mutant, protonation of the β-lactam nitrogen as the energetically preferred route (*17*) is expected to result in polarization and pronounced weakening of the β-lactam C−N bond. The decreased rate for acylation is, thus, entropically consistent with proton abstraction from the O−H group of serine-70 by a solvent molecule that is not optimally positioned as in the wt enzyme. Thus, identification by ENDOR of the sequestered water molecule in the active site affirms the importance of the glutamate-166 residue in the mechanism of TEM-1 β-lactamase. The ENDOR results also highlight the differences between catalytically competent and catalytically impaired active-site structures of the enzyme whereby mutation of the glutamate-166 residue (*13*, *58*) not only reduces the efficiency of acylation but also removes the important nucleophile required for hydrolytic breakdown of the acylenzyme.

ACKNOWLEDGMENT

We thank Dr. Wuyuan Lu for assistance in mass spectrometry, Dr. N. Strynadka and Professor M. N. G. James for communication of refined coordinates of the Glu166Asn acylenzyme, and Dr. E. V. Galtseva for helpful discussions and simulation of ENDOR spectra.

REFERENCES

1. Fleming, A. (1929) *Br. J. Pathol. 10*, 226−236.
2. Joris, B., Ghuysen, J. M., Dive, G., Renard, A., Dideberg, O., Charlier, P., Frère, J. M., Kelly, J., Boyington, J. C., Moews, P. C., and Knox, J. R. (1988) *Biochem. J. 250*, 313−324.
3. Bush, K., Jacoby, G. A., and Medeiros, A. A. (1995) *Antimocrob. Agents Chemother. 39*, 1211−1233.
4. Knox, J. R., Moews, P. C., and Frère, J. M. (1996) *Chem. Biol. 3*, 937−947.
5. Knox, J. R. (1995) *Antimicrob. Agents Chemother. 39*, 2593−2601.
6. Massova, I., and Mobashery, S. (1998) *Antimicrob. Agents Chemother. 42*, 1−17.
7. Wells, G. B., Mustafi, D., and Makinen, M. W. (1994) *J. Biol. Chem. 269*, 4577−4586.
8. Mustafi, D., and Makinen, M. W. (1994) *J. Biol. Chem. 269*, 4587−4595.
9. Makinen, M. W., Mustafi, D., and Kasa, S. (1998) Spin-Labeling IV: The Next Millennium. In *Biological Magnetic Resonance* (Berliner, L. J., Ed.) Vol. 14, pp 181−249, Plenum, New York.
10. Makinen, M. W. (1998) *Spectrochim. Acta A54*, 2269−2281.
11. Mustafi, D., and Makinen, M. W. (1995) *J. Am. Chem. Soc. 117*, 6739−6746.
12. Mustafi, D., Knock, M. M., Shaw, R. W., and Makinen, M. W. (1997) *J. Am. Chem. Soc. 119*, 12619−12628.
13. Adachi, H., Ohta, H., and Matsuzawa, H. (1991) *J. Biol. Chem. 266*, 3186−3191.
14. Strynadka, N. C. J., Adachi, H., Jensen, S. E., Johns, K., Sielecki, A., Betzel, C., Sutoh, K., and James, M. N. J. (1992) *Nature 359*, 700−705.
15. Osuna, J., Viadiu, H., Fink, A. L., and Soberon, X. (1995) *J. Biol. Chem. 270*, 775−780.
16. Ellerby, L. M., Escobar, W. A., Fink, A. L., Mitchison, C, and Wells, J. A. (1990) *Biochemistry 29*, 5797−5806.
17. Atanasov, B. P., Mustafi, D., and Makinen, M. W. (2000) *Proc. Natl. Acad. Sci. U.S.A. 97*, 3160−3165.
18. Sosa-Peinado, A., Mustafi, D., and Makinen, M. W. (2000) *Protein Expression Purif. 19*, 235−245.
19. Ho, S. N., Hunt, H. D., Horton, R. M., Pullen, J. K., and Pease, L. R. (1989) *Gene 77*, 51−59.
20. Smith, D. J., Maggio, E. T., and Kenyon, G. L. (1975) *Biochemistry 14*, 766−771.
21. Churg, A. H., Gibson, G., and Makinen, M. W. (1978) *Rev. Sci. Instrum. 49*, 212−214.
22. Makinen, M. W., Kuo, L. C., Dymowski, J. J., and Jaffer, S. (1979) *J. Biol. Chem. 254*, 356−366.
23. Maret, W., and Makinen, M. W. (1991) *J. Biol. Chem. 266*, 20636−20644.
24. Douzou, P. (1977) *Cryobiochemistry*, p 286, Academic Press, New York.
25. Douzou, P., Hui Bon Hoa, G., Maurel, P., and Travers, F. (1976) in *Handbook of Biochemistry and Molecular Biology* (Fasman, G. D., Ed.) 3rd ed., pp 520−540, Chemical Rubber Publishing Co., Cleveland.
26. Jiang, F. S., and Makinen, M. W. (1995) *Inorg. Chem. 34*, 1736−1744.
27. Mustafi, D., and Nakagawa, Y. (1994) *Proc. Natl. Acad. Sci. U.S.A. 91*, 11323−11327.
28. Turley, J. W., and Boer, F. P. B. (1972) *Acta Crystallogr., Sect. B 28*, 1641−1644.
29. Boles, M. O., Girven, R. J., and Gane, P. A. (1978) *Acta Crystallogr., Sect. B 34*, 461−466.
30. Jelsch, C., Maury, L., Masson, J. M., and Samama, J. P. (1993) *Proteins*: *Struct., Funct., Genet. 16*, 364−383.
31. Chiari, G., Fronczek, F. R., Davis, S. T., and Gandour, R. D. (1981) *Acta Crystallogr., Sect. B 37*, 1623−1625.
32. Rajeswaran, M., and Parthasarathy, R. (1985) *Acta Crystallogr., Sect. C 41*, 726−728.

33. Sutcliffe, J. G. (1978) *Proc. Natl. Acad. Sci. U.S.A. 75*, 3737−3741.
34. Nukaga, M., Tanimoto, K., Tsukamoto, K., Imajo, S., Ishiguro, M., and Sawai, T. (1993) *FEBS Lett. 332*, 93−98.
35. Scott, N., Hatlelid, K. M., MacKenzie, N. E., and Carter, D. E. (1993) *Chem. Res. Toxicol. 6*, 102−106.
36. Goldgur, Y., Dyda, F., Hickman, A. B., Jenkins, T. M., Craigie, R., and Davies, D. R. (1998) *Proc. Natl. Acad. Sci. U.S.A. 95*, 9150−9154.
37. Virden, R., Tan, A. K., and Fink, A. L. (1990) *Biochemistry 29*, 145−153.
38. Xaolin, Q., and Virden, R. (1996) *Biochem. J. 315*, 537−541.
39. Weston, G. S., Blazquez, J., Baquero, F., and Shoichet, B. K. (1998) *J. Med. Chem. 41*, 4577−4586.
40. Kiener, P. A., and Waley, S. G. (1978) *Biochem. J. 169*, 197−204.
41. Kuo, L. C., Fukuyama, J. M., and Makinen, M. W. (1983) *J. Mol. Biol. 163*, 63−103.
42. Rist, G. H., and Hyde, J. S. (1970) *J. Chem. Phys. 52*, 4633−4643.
43. Hurst, G. C., Henderson, T. A., and Kreilick, R. W. (1985) *J. Am. Chem. Soc. 107*, 7294−7299.
44. Mustafi, D., Sachleben, J. R., Wells, G. B., and Makinen, M. W. (1990) *J. Am. Chem. Soc. 112*, 2558−2566.
45. Mustafi, D., Joela, H., and Makinen, M. W. (1991) *J. Magn. Reson. 91*, 497−504.
46. Jiang, F., Tsai, S. W., Chen, S., and Makinen, M. W. (1998) *J. Phys. Chem. 102*, 4619−4627.
47. Mustafi, D., and Joela, H. (1995) *J. Phys. Chem. 99*, 11370−11375.
48. Narayana, P. A., Bowman, M. K., Becker, D., and Kevan, L. (1977) *J. Chem. Phys. 67*, 1990−1996.
49. Wells, G. B., and Makinen, M. W. (1988) *J. Am. Chem. Soc. 110*, 6343−6352.
50. Lee, B., and Richards, F. M. (1971) *J. Mol. Biol. 55*, 379−400.
51. Chothia, C. (1984) *Annu. Rev. Biochem. 53*, 537−572.
52. Bürgi H. B., Dunitz, J. D., and Shafter, E. (1974) *Acta Crystallogr., Sect. B 30*, 1517−1527.
53. Hyde, J. S., Rist, G. H., and Eriksson, L. E. G. (1968) *J. Phys. Chem. 72*, 4269−4276.
54. Strynadka, N. C. J., Martin, R, Jensen, S. E., Gold, M., and Jones, J. B. (1996) *Nat. Struct. Biol. 3*, 688−695.
55. Damblon, C., Raquet, X., Lian, L. Y., Lamotte-Brasseur, J., Fonze, E., Charlier, P., Roberts, G. C. K., and Frère, J. M. (1996) *Proc. Natl. Acad. Sci. U.S.A. 93*, 1747−1752.
56. Zawadzke, L. E., Chen, C. C. H., Banerjee, S., Li, Z., Wäsch, S., Kapadia, G., Moult, J., and Herzberg, O. (1996) *Biochemistry 35*, 16475−16482.
57. Guillaume, G, Vanhove, M., Lamotte-Brasseur, J., Ledent, P., Jamin, M., Joris, B., and Frère, J. M. (1997) *J. Biol. Chem. 272*, 5438−5444.
58. Knox, J. R., Moews, P. C., Escobar, W. A., and Fink, A. L. (1993) *Protein Eng. 6*, 11−18.

BI0021075